JACS
JOURNAL OF THE AMERICAN CHEMICAL SOCIETY

Communication

pubs.acs.org/JACS

Water Oxidation Electrocatalyzed by an Efficient $Mn_3O_4/CoSe_2$ Nanocomposite

Min-Rui Gao, Yun-Fei Xu, Jun Jiang, Ya-Rong Zheng, and Shu-Hong Yu*

Division of Nanomaterials and Chemistry, Hefei National Laboratory for Physical Sciences at Microscale, Department of Chemistry, National Synchrotron Radiation Laboratory, University of Science and Technology of China, Hefei, Anhui 230026, The People's Republic of China

Supporting Information

ABSTRACT: The design of efficient, cheap, and abundant oxygen evolution reaction (OER) catalysts is crucial to the development of sustainable energy sources for powering fuel cells. We describe here a novel $Mn_3O_4/CoSe_2$ hybrid which could be a promising candidate for such electrocatalysts. Possibly due to the synergetic chemical coupling effects between Mn_3O_4 and $CoSe_2$, the constructed hybrid displayed superior OER catalytic performance relative to its parent $CoSe_2$/DETA nanobelts. Notably, such earth-abundant cobalt (Co)-based catalyst afforded a current density of 10 mA cm^{-2} at a small overpotential of ~0.45 V and a small Tafel slope down to 49 mV/decade, comparable to the best performance of the well-investigated cobalt oxides. Moreover, this $Mn_3O_4/CoSe_2$ hybrid shows good stability in 0.1 M KOH electrolyte, which is highly required to a promising OER electrocatalyst.

The supersession of noble metal catalysts by earth-abundant and inexpensive materials is particularly needed for the oxygen evolution reaction (OER) which plays an important role in many electrochemical processes such as solar fuel production (water splitting).[1] Currently, the commonly used catalysts for OER in electrolysis cells are still ruthenium (Ru) and iridium (Ir) oxides, although these metals are among the rarest elements in Earth's crust.[2] Therefore, searching for alternative catalysts which provide the availability for large-scale application and also high efficiency are critical to viable water electrolytic systems.

Over the last few decades, various cobalt (Co)-based OER catalysts have been designed for water oxidation potential, including nanostructured Co_3O_4 and Co_3O_4-based hybrids,[3] Co_2O_3 nanoparticles (NPs),[4] amorphous cobalt-phosphate-based material (Co-Pi),[1b,5] Co-Pi/α-Fe_2O_3 composites,[6] Co-OEC (oxygen evolving complex),[7] Co(III) hangman β-octafluoro corroles,[8] $[Co_4(H_2O)_2(PW_9O_{34})_2]^{10-}$,[1a,9] $NiCo_2O_4$ aerogels,[10] and so on. In addition to abundance and low cost, these Co-based materials can often generate O_2 under mild reaction conditions and modest overpotentials. More excitingly, recent studies show that the OER performance of Co-based catalysts can be greatly improved by incorporating other functional materials.[3e,f,6] For instance, Gamelin et al. reported integration of Co-Pi OER catalyst with α-Fe_2O_3 can reduce the external power for catalyst's electrolysis chemistry,[6] and the intrinsic reasons for such enhancement were interpreted by Barroso and co-workers recently.[11] The groups of Bell[3e] and Dai[3f] reported the OER activity of Co_3O_4 nanocrystals was significantly enhanced by anchoring them on Au and graphene support, respectively. It is believed that the synergetic chemical coupling effects between Co-based catalysts and foreign materials presumably lead to the substantial enhancement.

Herein, based on our previous studies,[12] we report that another kind of Co-based nanomaterials, ultrathin lamellar mesostructured $CoSe_2$/DETA (DETA = diethylenetriamine) nanobelts can display certain electrocatalytic activity for water oxidation in alkaline medium. Several advantages of such Co-based catalyst are worth highlighting: abundant and affordable material for large-scale utilization, large BET surface area of 77 m^2 g^{-1} that can provide enough active sites and is homogeneously distributed, copious surface amino groups that allow loading of highly dispersed foreign materials.[12c] By a simple polyol reduction method, we have successfully grown and anchored Mn_3O_4 NPs, a material with little OER activity by itself, on $CoSe_2$/DETA nanobelts. Notably, the resulting $Mn_3O_4/CoSe_2$ hybrid displays good stability and also excellent OER electrocatalytic activity with high current and small overpotential (~0.45 V) at a current density of 10 mA cm^{-2}.

Ultrathin $CoSe_2$/DETA nanobelts were first prepared in high yield by a facile solvothermal strategy reported previously.[12a] Then, Mn_3O_4 NPs were anchored on the surface of $CoSe_2$/DETA nanobelts through an effective polyol reduction approach recently developed by Cai et al. (see Supporting Information (SI) for details of the synthesis).[13] Figure 1a–c shows transmission electron microscopy (TEM) images of $Mn_3O_4/CoSe_2$ hybrid with different magnifications. One striking feature is that the obtained hybrid material is flexible, thin, and almost transparent, just as the original $CoSe_2$ nanobelts used. The Mn_3O_4 NPs with an average size of ~15.7 nm are fairly well decorated on the backbone of $CoSe_2$ nanobelts (Figure 1b and inset). The selected-area electron diffraction (SAED) pattern (inset in Figure 1c) shows three discernible rings indexed to (103), (004), (321) planes of tetragonal Mn_3O_4 (JCPDS 24-0734), and also diffraction peaks of the $CoSe_2$ matrix can be clearly detected (marked by yellow arrows). High resolution TEM (HRTEM) investigation in Figure 1d shows resolved lattice fringes of Mn_3O_4 (103) planes with a spacing of 2.76 Å, as well as (220) planes of neighboring

Received: December 9, 2011
Published: January 26, 2012

dx.doi.org/10.1021/ja211526y | J. Am. Chem.Soc. 2012, 134, 2930–2933

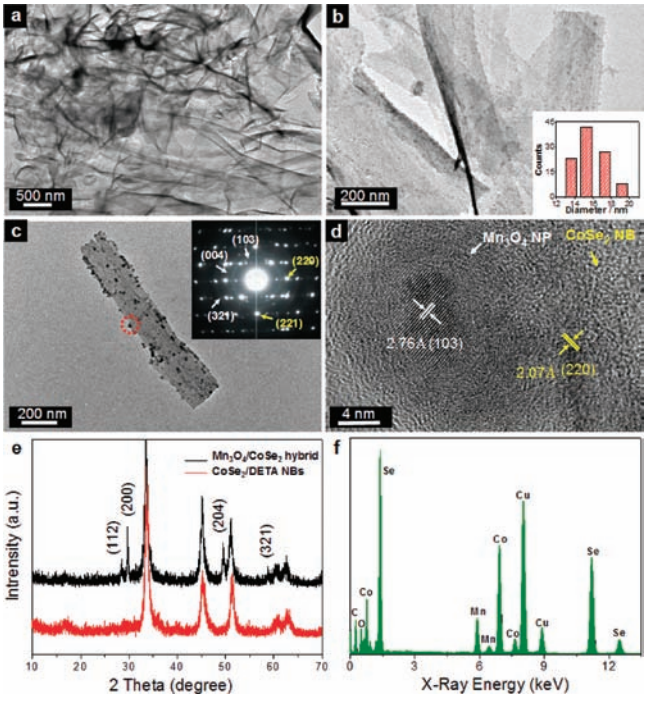

Figure 1. (a–c) TEM images with different magnifications of Mn_3O_4/$CoSe_2$ hybrid prepared at 278 °C for 1 h. The inset in (b) shows the corresponding particle-size histogram, and that in (c) the corresponding SAED pattern. (d) HRTEM image of an attached nanoparticle and its neighboring support taken on the marked part in (c). (e) XRD patterns and (f) EDX spectrum of the hybrid.

$CoSe_2$ support with a spacing of 2.07 Å. The above results are well consistent with the mixed phases checked by X-ray diffraction (XRD) technique (Figure 1e). Energy-dispersive X-ray spectroscopy (EDS) further confirms the formation of Mn_3O_4/$CoSe_2$ hybrid, where only Mn, O, Co, and Se can be detected with Cu and C peaks emanating from the carbon-coated TEM grid (Figure 1f). The Mn_3O_4 loading amount was about 45.8 wt % based on the amounts of $Mn(acac)_3$ and $CoSe_2$/DETA precursors used in the synthesis.

Anchoring of Mn_3O_4 NPs on the $CoSe_2$/DETA surface was easily achieved via a heterogeneous nucleation process, as shown in Scheme 1a. Almost no free Mn_3O_4 NPs were found in solution (Figure 1b,c) where homogeneous nucleation will take

Scheme 1. Schematic Illustration Showing Two Different Growth Behaviors of Mn_3O_4[a]

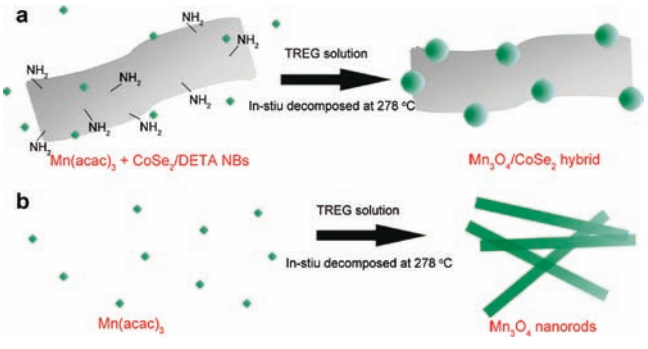

[a](a) Polyol synthesis with $CoSe_2$/DETA NBs to generate Mn_3O_4/$CoSe_2$ hybrid. (b) Polyol synthesis without $CoSe_2$/DETA NBs, leading to aggregated Mn_3O_4 NRs.

effect. The confined growth of Mn_3O_4 on the $CoSe_2$/DETA surface was attributed to the copious amino groups on the $CoSe_2$/DETA surface (SI, Figure S1), which can serve as nucleation sites to couple Mn precursors and lead to corresponding Mn_3O_4 deposition on $CoSe_2$ under the thermal reduction condition.[12b] The FT-IR spectrum shows that no DETA molecules remain on the obtained Mn_3O_4/$CoSe_2$ hybrid (SI, Figure S1), which should be the result of both Mn_3O_4 coverage and the high-temperature reaction. In contrast, the exact same synthesis strategy produced aggregated Mn_3O_4 nanorods (NRs) with a diameter of ~100 nm and lengths up to several micrometers in the absence of $CoSe_2$ (Scheme 1b and SI, Figure S2). Such amazing morphological difference highlights the important role of $CoSe_2$ NBs as a useful support for mediating the growth of other functional nanomaterials.

To appraise the catalytic properties of the new Mn_3O_4/$CoSe_2$ hybrid nanobelts for electrochemical oxidation of water to oxygen, film of Mn_3O_4/$CoSe_2$ hybrid was prepared onto glassy carbon electrodes for cyclic voltammetry (CV) in O_2-saturated 0.1 M KOH (see SI for experimental details). Similar measurements for bare glassy carbon (GC) electrode, pure $CoSe_2$/DETA nanobelts, Mn_3O_4 nanorods, and Pt/C reference (Johnson-Matthey, 20-wt %) were also performed for comparison. Potentials are reported versus Ag/AgCl (measured) or the reversible hydrogen electrode (RHE, see SI for RHE calibration). Figure 2a shows their linear sweeps in an anodic direction, from which we can see that the Mn_3O_4/$CoSe_2$

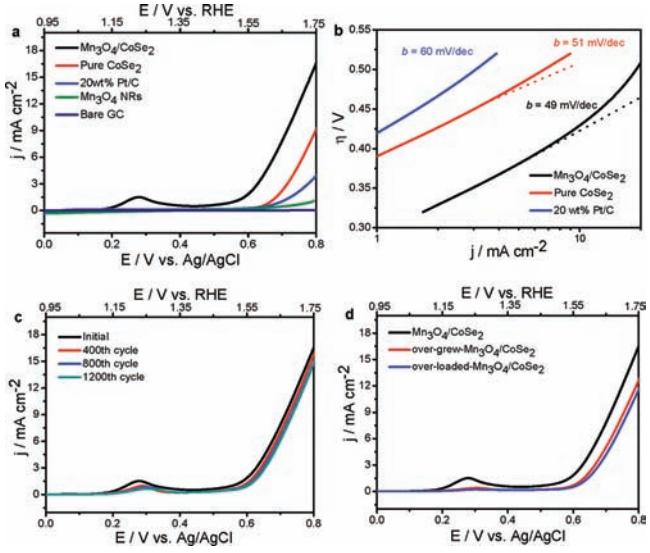

Figure 2. (a) Polarization curves for OER on bare GC electrode and modified GC electrodes comprising the Mn_3O_4 NRs, 20 wt % Pt/C, pure $CoSe_2$/DETA NBs, and Mn_3O_4/$CoSe_2$ hybrid, respectively. (b) Tafel plot (overpotential versus log current) derived from (a). (c) OER polarization curves for the Mn_3O_4/$CoSe_2$ hybrid before and after different cycles of accelerated stability test. (d) OER polarization curves for the Mn_3O_4/$CoSe_2$ hybrid, overgrown-Mn_3O_4/$CoSe_2$ hybrid, and overloaded-Mn_3O_4/$CoSe_2$ hybrid, respectively. All the measurements were performed in O_2-purged 0.1 M KOH (pH ~13). Catalyst loading: ~0.2 mg cm^{-2}. Sweep rate: 5 mV s^{-1}.

hybrid exhibits greater current and earlier onset of catalytic current as compared with pure $CoSe_2$/DETA nanobelts and Pt/C reference (also see CV analyses in the SI, Figure S3). By contrast, bare GC electrode does not affect OER activity. The current density of 10 mA cm^{-2}, which is a metric relevant to

dx.doi.org/10.1021/ja211526y | J. Am. Chem.Soc. 2012, 134, 2930–2933

solar fuel synthesis,[14] can be achieved at a small overpotential (η) of ~0.45 V for our constructed catalyst, comparable to the performance of the best reported Co_3O_4/graphene catalyst at the similar loading (0.2 mg cm^{-2}).[3f] Of note, the free Mn_3O_4 NRs synthesized without $CoSe_2$ only affect little OER activity (Figure 2a). To test whether Mn_3O_4 NPs but not NRs can possess OER activity, we prepared two kinds of Mn_3O_4 NPs with different particle sizes from the literatures and still no OER activity can be found (SI, Figure S4). It is thus deduced that the excellent OER activity of $Mn_3O_4/CoSe_2$ hybrid was originated from $CoSe_2$/DETA NBs, where Mn_3O_4 served as a synergist. Figure 2b shows that the Tafel slope of $Mn_3O_4/CoSe_2$ hybrid is ~49 mV/decade, which is smaller than that of pure $CoSe_2$ NBs and previously reported Co-based OER catalysts such as Co_3O_4 and Co_3O_4/graphene at similar loading.[3a,f] In addition, the new $Mn_3O_4/CoSe_2$ hybrid catalyst also exhibited high stability for OER. Figure 2c shows that, after 1200 potential cycles, the $Mn_3O_4/CoSe_2$ hybrid almost afforded the same *j*-V curves as initial catalyst, only with negligible drops of the anodic current (also see the SI, Figure S5).

As to cobalt oxides, it has been well documented that Co^{IV} cations are particularly important to enable OER.[3e,15] The role of Co^{IV} species for the electrochemical oxidation of water in base was proposed by Bell et al. in a recent work.[3e] As schemed in SI, Figure S6 (which was adapted from ref 3e), reaction 3 is hypothesized as rate-limiting step. The presence of Co^{IV} cations was believed to enhance the electrophilicity of the adsorbed O and thus to facilitate the formation of O−OH via nucleophilic attack, which was also believed to promote the deprotonation of the OOH species, via electron-withdrawimg inductive effect, to produce O_2.[3e] In the case of ultrathin $CoSe_2$ NBs, the surface Co^{IV} cations, which were verified by the binding energy of Co $2p_{3/2}$ at 778.5 eV[16] (Figure 3), presumably are the cause of their OER activity. In support of this interpretation, we

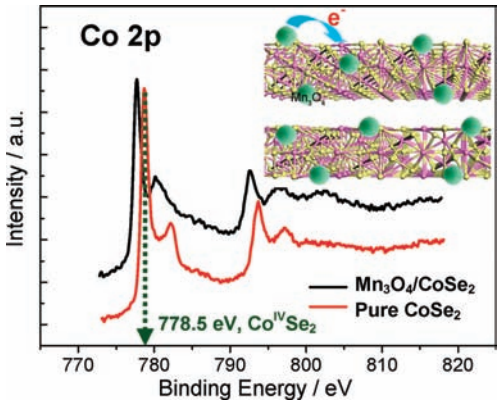

Figure 3. Co 2p XPS spectra for pure $CoSe_2$/DETA NBs and as-constructed $Mn_3O_4/CoSe_2$ hybrid. Inset demonstrates the electron donation from the Mn_3O_4 to $CoSe_2$. Pink and yellow balls correspond to Co and Se atoms, respectively.

designed an experiment to cover $CoSe_2$ surface and then assessed corresponding OER activity. As shown in SI, Figure S7, two samples, that is, overloaded-$Mn_3O_4/CoSe_2$ and overgrown-$Mn_3O_4/CoSe_2$ hybrids, could be obtained by doubling the Mn precursor feed and increasing the reaction temperature to 290 °C, respectively. It can be clearly seen that a large part of $CoSe_2$ surfaces is sheltered by OER-inactive Mn_3O_4 for the two samples. The OER performances of the two samples as well as previously obtained $Mn_3O_4/CoSe_2$ catalyst were compared in Figure 2d. In the same condition, the two samples exhibited lower OER currents than previously obtained $Mn_3O_4/CoSe_2$ catalyst. Furthermore, the two samples afforded a current density of 10 mA cm^{-2} at overpotentials of ~0.49 and 0.51 V, respectively, which are larger than that of ~0.45 V for previously obtained $Mn_3O_4/CoSe_2$ catalyst. These results indicate that the large exposure of surface Co is essential to the electrochemical evolution of oxygen.

It is interesting to understand the intrinsic reason of enhanced OER property of $CoSe_2$/DETA NBs after anchoring Mn_3O_4 NPs. Because the surface Co^{IV} cations are active centers for OER catalysts,[3e] it will be helpful to study the electronic structure of Co in the $Mn_3O_4/CoSe_2$ catalyst. Figure 3 compares the X-ray photoelectron spectroscopy (XPS) data of pure $CoSe_2$/DETA and $Mn_3O_4/CoSe_2$ catalysts. It can be seen that the electron binding energy of Co 2p has a ~0.84 eV decrease after loading with Mn_3O_4. Such a big shift in binding energy is probably due to electron transfer from Mn_3O_4 to $CoSe_2$, which can be further confirmed by the normalized X-ray absorption near edge spectra (XANES) of the two catalysts collected at Co K edge (see SI, Figure S8). Similar electron donation from metal oxides to noble metals such as platinum (Pt) was often observed, and the modified electronic structure of Pt upon its synergistic interaction with the metal oxides can result in an enhanced catalytic property.[17] In the case of $Mn_3O_4/CoSe_2$ catalyst, the electron donation from Mn_3O_4 to $CoSe_2$ will make Mn_3O_4 more acidic (Lewis acid), which facilitates the activation of H_2O (Lewis base) molecules through Lewis acid−base interaction, thus leading to the improved OER activity of the hybrid catalyst. A real understanding of the synergistic enhancement of OER activity observed experimentally is ongoing.

In summary, we have reported that a novel $Mn_3O_4/CoSe_2$ hybrid nanocomposite catalyst can be synthesized by a simple polyol reduction route. This inexpensive, earth-abundant, and easily constructed catalyst exhibited excellent OER electrochemical activity with a small overpotential of ~0.45 V at the current density of 10 mA·cm^{-2} and large anodic currents in alkaline medium. Furthermore, the accelerated tests of $Mn_3O_4/CoSe_2$ hybrid catalyst revealed its good durability. Our studies raise promising possibilities for designing effective OER electrocatalysts by synergistic coupling of nonprecious functional materials, which is highly required for energy conversion technologies.

■ ASSOCIATED CONTENT

Ⓢ Supporting Information

Full synthetic procedures, details of electrochemical measurements, RHE calibration, and FT-IR, XRD, TEM, HRTEM, additional electrochemical data. This material is available free of charge via the Internet at http://pubs.acs.org.

■ AUTHOR INFORMATION

Corresponding Author

shyu@ustc.edu.cn.

Notes

The authors declare no competing financial interest.

■ ACKNOWLEDGMENTS

We acknowledge the funding support from the National Basic Research Program of China (2010CB934700), the National

Natural Science Foundation of China (Nos. 91022032, 21061160492, 50732006, J1030412), and International Science & Technology Cooperation Program of China (2010DFA41170), and the Principal Investigator Award by the National Synchrotron Radiation Laboratory at the University of Science and Technology of China.

REFERENCES

(1) (a) Yin, Q.; Tan, J. M.; Besson, C.; Geletii, Y. V.; Musaev, D. G.; Kuznetsov, A. E.; Luo, Z.; Hardcastle, K. I.; Hill, C. L. *Science* **2010**, *328*, 342. (b) Kanan, M. W.; Nocera, D. G. *Science* **2008**, *321*, 1072.

(2) (a) Petrykin, V.; Macounova, K.; Shlyakhtin, O. A.; Krtil, P. *Angew. Chem., Int. Ed.* **2010**, *49*, 4813. (b) Frame, F. A.; Townsend, T. K.; Chamousis, R. L.; Sabio, E. M.; Dittrich, T.; Browning, N. D.; Osterloh, F. E. *J. Am. Chem. Soc.* **2011**, *133*, 7264.

(3) (a) Esswein, A. J.; McMurdo, M. J.; Ross, P. N.; Bell, A. T.; Tilley, T. D. *J. Phys, Chem. C* **2009**, *113*, 15068. (b) Jiao, F.; Frei, H. *Angew, Chem., Int. Ed.* **2009**, *48*, 1841. (c) Jiao, F.; Frei, H. *Energy Environ. Sci.* **2010**, *3*, 1018. (d) Lu, B.; Cao, D.; Wang, P.; Wang, G.; Gao, Y. *Int. J. Hydrogen Energy* **2011**, *36*, 72. (e) Yeo, B. S.; Bell, A. T. *J. Am. Chem. Soc.* **2011**, *133*, 5587. (f) Liang, Y.; Li, Y.; Wang, H.; Zhou, J.; Wang, J.; Regier, T.; Dai, H. *Nat. Mater.* **2011**, *10*, 780. (g) Qiao, Y.; Li, C. M. *J. Mater. Chem.* **2011**, *21*, 4027. (h) Zhou, Q.; Li, C. M.; Li, J.; Cui, X. Q.; Gervasio, D. *J. Phys. Chem. C* **2007**, *111*, 11216. (i) Zhou, Q.; Li, C. M.; Li, J.; Lu, J. T. *J. Phys. Chem. C* **2008**, *112*, 18578.

(4) Wee, T. L.; Sherman, B. D.; Gust, D.; Moore, A. L.; Moore, T. A.; Liu, Y.; Scaiano, J. C. *J. Am. Chem. Soc.* **2011**, *133*, 16742.

(5) (a) Surendranath, Y.; Dincă, M.; Nocera, D. G. *J. Am. Chem. Soc.* **2009**, *131*, 2615. (b) Lutterman, D. A.; Surendranath, Y.; Nocera, D. G. *J. Am. Chem. Soc.* **2009**, *131*, 3838.

(6) (a) Zhong, D. K.; Sun, J. W.; Inumaru, H.; Gamelin, D. R. *J. Am. Chem. Soc.* **2009**, *131*, 6086. (b) Zhong, D. K.; Gamelin, D. R. *J. Am. Chem. Soc.* **2010**, *132*, 4202.

(7) Reece, S. Y.; Hamel, J. A.; Sung, K.; Jarvi, T. D.; Esswein, A. J.; Pijpers, J. J. H.; Nocera, D. G. *Science* **2011**, *334*, 645.

(8) Dogutan, D. K. Jr.; R., M.; Nocera, D. G. *J. Am. Chem. Soc.* **2011**, *133*, 9178.

(9) Hurst, J. K. *Science* **2010**, *328*, 315.

(10) Chien, H. C.; Cheng, W. Y.; Wang, Y. H.; Wei, T. Y.; Lu, S. Y. *J. Mater. Chem.* **2011**, *21*, 18180.

(11) Barroso, M.; Cowan, A. J.; Pendlebury, S. R.; Grätzel, M.; Klug, D. R.; Durrant, J. R. *J. Am. Chem. Soc.* **2011**, *133*, 14868.

(12) (a) Gao, M. R.; Yao, W. T.; Yao, H. B.; Yu, S. H. *J. Am. Chem. Soc.* **2009**, *131*, 7486. (b) Gao, M. R.; Liu, S.; Jiang, J.; Cui, C. H.; Yao, W. T.; Yu, S. H. *J. Mater. Chem.* **2010**, *20*, 935. (c) Gao, M. R.; Gao, Q.; Jiang, J.; Cui, C. H.; Yao, W. T.; Yu, S. H. *Angew. Chem., Int. Ed.* **2011**, *50*, 4905.

(13) (a) Cai, W.; Wan, J. Q. *J. Colloid Interface Sci.* **2007**, *305*, 366. (b) Wan, J. Q.; Cai, W.; Meng, X. X.; Liu, E. Z. *Chem. Commun.* **2007**, 5004.

(14) Matsumoto, Y.; Sato, E. *Mater. Chem. Phys.* **1986**, *14*, 397.

(15) (a) Lyons, M. E. G.; Brandon, M. P. *Int. J. Electrochem. Soc.* **2008**, *3*, 1425. (b) Chou, N. H.; Ross, P. N.; Bell, A. T.; Tilley, T. D. *ChemSusChem* **2011**, *4*, 1566.

(16) NIST X-ray Photoelectron Spectroscopy Database. http://srdata.nist.gov/xps/EngElmSrchQuery.aspx?EType=PE&CSOpt=Retri_ex_dat&Elm=Co.

(17) (a) Bahl, M. K.; Tsai, S. C.; Chung, Y. W. *Phys. Rev. B* **1980**, *21*, 1344. (b) Ho, V. T. T.; Pan, C. J.; Rick, J.; Su, W. N.; Hwang, B. J. *J. Am. Chem. Soc.* **2011**, *133*, 11716. (c) Wang, C.; Daimon, H.; Sun, S. H. *Nano Lett.* **2009**, *9*, 1493.